JACS
JOURNAL OF THE AMERICAN CHEMICAL SOCIETY

Article

pubs.acs.org/JACS

Design, Synthesis, and Properties of Phthalocyanine Complexes with Main-Group Elements Showing Main Absorption and Fluorescence beyond 1000 nm

Taniyuki Furuyama, Koh Satoh, Tomofumi Kushiya, and Nagao Kobayashi*

Department of Chemistry, Graduate School of Science, Tohoku University, Sendai 980-8578, Japan

Supporting Information

ABSTRACT: We present a comprehensive description of the unique properties of newly developed phthalocyanines (Pcs) containing main-group elements that absorb and emit in the near-IR region. Group 16 (S, Se, and Te) elements and group 15 (P, As, and Sb) elements were used as peripheral and central (core) substituents. With the introduction of group 16 elements into free-base Pc, a red-shift of the Q-band was observed, as a result of the electron-donating ability of group 16 elements particularly at the α positions. An X-ray crystallographic analysis of α-ArS-, ArSe-, and ArTe-linked free-base Pcs was also successfully performed, and the relationship between structure and optical properties was clarified. When a group 15 element ion was introduced into the center of the Pc ring, the resulting Pcs showed a single Q-band peak beyond 1000 nm (up to 1056 nm in CH_2Cl_2). In particular, $[(ArS)_8PcP(OMe)_2]^+$ and $[(ArS)_8PcAs(OMe)_2]^+$ exhibited a distinct fluorescence in the 960−1400 nm region with moderate quantum yields. The atomic radius of the group 15 element is important for determining the Pc structure, so that this can be controlled by the choice of group 15 elements. Electrochemical data revealed, while MO calculations suggested, that the red-shift of the Q-band is attributable to a decrease of the HOMO−LUMO gap due to significant and moderate stabilization of the LUMO and HOMO, respectively. The effect of peripheral substutuents and a central P(V) ion on the Q-band shift was independently predicted by MO calculations, while the magnitude of the total calculated shift was in good agreement with the experimental observations. The combination of spectral, electrochemical, and theoretical considerations revealed that all of the central group 15 elements, peripheral group 16 elements, and their positions are necessary to shift the Q-band beyond 1000 nm, indicating that the substitution effects of group 15 and 16 elements act synergistically. The Pcs having Q-bands beyond 1000 nm in this study also had stability under aerobic conditions comparative to that of CuPc, which is presently being widely used in consumer products.

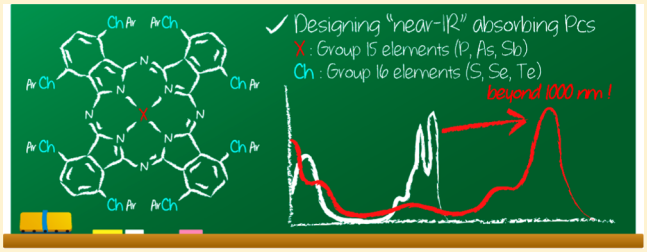

INTRODUCTION

Various types of organic dye have been isolated from natural products, while many artificially designed dyes have been synthesized to date for various purposes, including functional materials and light-harvesting.[1] Phthalocyanines (Pcs) having a symmetrical 18π electron aromatic macrocycle, which is closely related to the naturally occurring porphyrins, are one of the most well-known and successful artificial dyes (Figure 1a). In particular, Pcs absorbing in the near-infrared (near-IR) region are desired in various fields, such as organic solar cells, photodynamic therapy of cancer, heat absorbers, and near-IR imaging. Figure 1b shows a typical electronic absorption spectrum of metalated Pc. The majority of these applications take advantage of the unique optical (specifically Q-band) properties of Pcs, which can be fine-tuned using appropriate peripheral substitutions.[2]

In the chemistry of Pcs, designing the envelope of their Q-band is one of the most interesting and essential topics. A number of theoretical studies of the absorption properties have also been reported, while one textbook on hitherto-reported absorption spectra of Pcs was edited by our group in 2010.[3] Thus, substantial knowledge for rationally designing new Pc derivatives has now been compiled experimentally and theoretically. On the basis of the reported literature, three common approaches exist for tailoring the Pc derivatives absorbing in the near-IR region. (1) Extending the π conjugation by benzoannulation and/or expansion of the macrocycle results in a decrease in separation between the HOMO and LUMO energies, which inevitably leads to red-shifted spectra.[4,5] (2) Oligomerization of Pcs is also effective because orbital interaction between monomeric Pc molecules can extend the electronic conjugation. Recently Fukuda, Ishikawa, and co-workers reported that the Q-band of the oxidized species of a quadruple-decker Pc extended into the IR region.[6] (3) The last approach is lowering of molecular symmetry, which leads to splitting of the Q-band.[2e,7] However, these "π electron-modified" approaches have several disadvantages. For example, benzoannulated Pcs are prone to oxidation, and hence are sensitive to air. Azulene-fused Pc is relatively

Received: October 28, 2013
Published: December 13, 2013

dx.doi.org/10.1021/ja411016f | J. Am. Chem. Soc. 2014, 136, 765−776

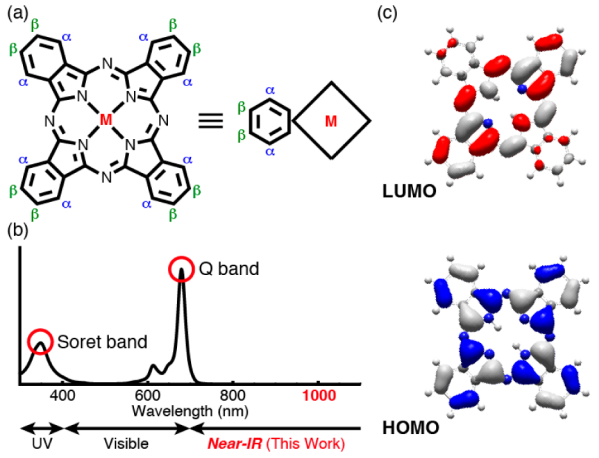

Figure 1. (a) Molecular structure of Pc. (b) Typical absorption spectrum of a metalated Pc with D_{4h} symmetry. (c) Frontier orbitals of an unsubstituted free-base Pc.

stable, but the shape of the Q-band envelope is completely different from that of the original Pc (i.e., weak).[8] Separation of low-symmetry Pcs is difficult, and the yield is low. On the other hand, the reaction sequences leading to discrete oligomers are relatively long and tedious, and the final yield is usually very low. Hence, no Pc derivatives having a sharp Q-band in the region beyond 1000 nm have been reported to date, and the development of a new strategy in this regard has been awaited as the next breakthrough in the chemistry of not only Pcs, but also organic functional dyes.

To overcome this problem, we have chosen main-group (groups 15 and 16) elements as substituents. These elements have notable features, such as effective orbital interactions, diversity of coordination, and large electronegativity[9] so that their introduction into Pcs can change the spectrum significantly (Scheme 1). In our communication in 2011, we

Scheme 1. Molecular Design of Near-IR Absorbing Pcs

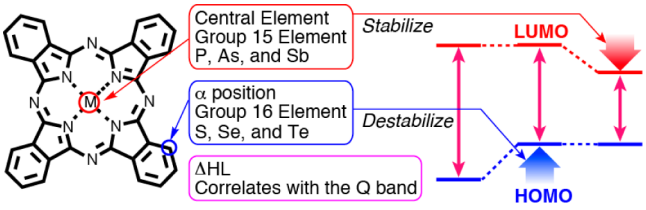

reported, based on this concept, phosphorus(V) complexes of α-substituted (S and Se) Pcs having their main absorptions beyond 1000 nm.[10] Herein, we first discuss the synthesis and properties of group 16 (S, Se, and Te)-substituted free-base Pcs at α-positions in detail, and then describe Pcs containing group 15 elements (P, As, and Sb) in their center, to classify the effect of these elements. Pc complexes with group 15 elements are still rare;[11−13] in particular, the first arsenic(V) complex was reported in 2012 only as a mixture of isomers by Isago.[14] In this work, we chose Pcs having high symmetry to avoid the effect of regioisomers and to reveal the absorption, emission, and electronic properties as unambiguously as possible.

RESULTS AND DISCUSSION

1. Effect of Electron-Rich Group 16 Elements. *Synthesis.* It is important to obtain the free-base form of a Pc, because it is this form that provides easy access to complexes containing various central elements. Representative procedures of free-base (metal-free) Pcs[15] containing group 16 (S, Se, and Te) elements are shown in Scheme 2. Free-base Pcs **3a−c** can

Scheme 2. Synthesis of α-Chalcogenyl Free-Base Pcs[a]

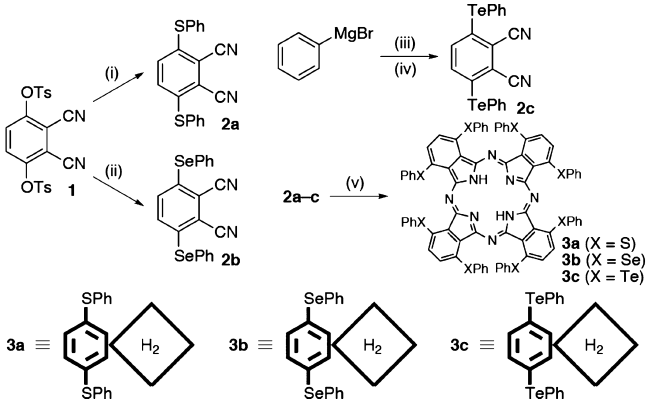

[a]Reagents and conditions: (i) PhSH (4 equiv), K_2CO_3 (4 equiv), DMSO, room temperature, 14 h, 66%; (ii) PhSeSePh (1.4 equiv), $NaBH_4$ (30 equiv), DMSO, room temperature, 3 h, 37%; (iii) Te (1 equiv), THF, room temperature, 2 h; (iv) **1** (0.25 equiv), THF, room temperature, 1 h, 64% (based on **1**); (v) ^{n}BuOLi, ^{n}BuOH, reflux, 2 h, 74% (for **3a**), 57% (for **3b**), 32% (for **3c**).

be prepared in moderate yields from the corresponding phthalonitriles via cyclotetramerization using the lithium method.[2d] Phthalonitriles **2a−c** were prepared from the same precursor **1** and chalcogenyl anions via S_NAr reaction. In the case of aryl-substituted chalcogenyl phthalonitriles, chalcogenyl anions were generated rationally using a Grignard reagent and elemental form of chacogenyl atom. This method is applicable to functionalized aryl metal species, and several Pcs were obtained therefrom. All Pcs were characterized by ^{1}H NMR and HR-MALDI-FT-ICR-MS spectroscopy. These compounds exhibit good solubility in organic solvents and good stability in air-saturated solution under ambient light.

Optical Properties. As shown in Figure 2, the Q_{00} bands of α-PhX−Pcs **3a−c** appear at 809, 811, and 835 nm in $CHCl_3$, respectively. All Pcs can absorb strongly in the near-IR region, so that the spectral differences cannot be recognized directly by the appearance of solution colors seen by the human naked eye. For example, the color of a solution of **3a** is pale red rather than the typical blue-green color of Pc [Figure S1 in the Supporting Information]. As reported for the spectra of naphthalocyanines and related Pcs absorbing in the 750−800 nm region,[4a] the Q-bands of **3a−c** might be split theoretically into four peaks, but they show only two peaks (Q_{00} and Q_{01} bands). The MCD spectra give additional information about the shape of the Q-bands, that is, excited states. Dispersion-type signals were observed corresponding to the Q_{00} bands of **3a−c**. It is considered that the splitting of the Q-band is so small that the superimposition of two oppositely signed Faraday *B* terms gave seemingly *A* term-like MCD signals, the so-called pseudo Faraday *A* term. Notably, the position of the Q-bands exhibits a correlation with the electronegativity of the chalcogenyl elements. Hence, the introduction of group 16 elements does not affect the π-conjugation structure of Pc, but only shifts the Q-bands to the red, depending on the electron-donating ability of the group 16 element.

dx.doi.org/10.1021/ja411016f | J. Am. Chem. Soc. 2014, 136, 765−776

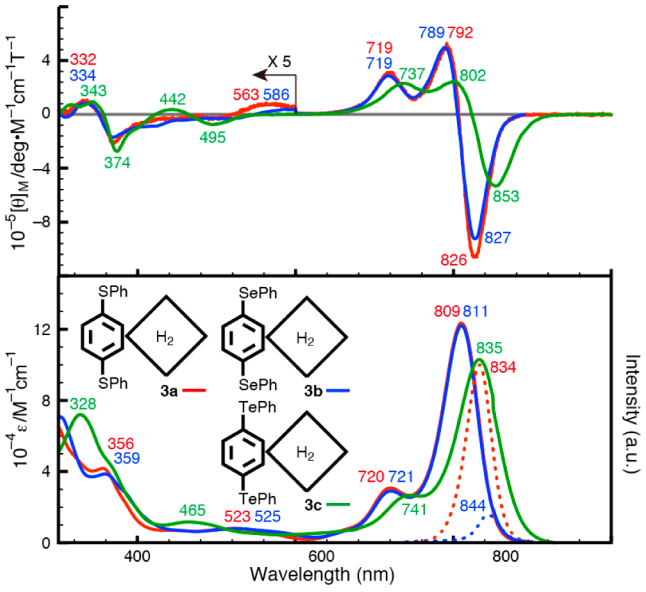

Figure 2. UV−vis−NIR absorption (bottom, solid lines), emission (bottom, dotted lines), and MCD (top) spectra of **3a** (red), **3b** (blue), and **3c** (green) in $CHCl_3$.

When excited at the Q_{01} band, compounds **3a** and **3b** showed a weak fluorescence in the near-IR region (peaks at 834 and 844 nm, and Φ_{FL} = 0.045 and 0.007, respectively) with a small Stokes shift (370 and 480 cm^{-1}, respectively), while fluorescence was not observed for compound **3c**. The fluorescence of **3a** and **3b** appears to result from the rigid structure of the Pc core, while the fluorescence of **3c** might be quenched by the heavy atom effect of the tellurium atoms.

Solid-State Structures of α-Chalcogenyl Pcs. To examine the structural relationship between group 16 elements at α-positions and their Pcs, X-ray crystallographic analysis was carried out. Unfortunately, because suitable single crystals of **3a** and **3c** could not be obtained, we tried to obtain single crystals of other chalcogenyl Pcs substituted by different aryl groups. Finally, desired crystals were obtained with respect to 2,6-dimethylphenyl substituted Pc (for S, **3d**) and 2,4,6-trimethylphenyl substituted Pc (for Te, **3e**). The X-ray crystallographic structures of α-chalcogenyl free-base Pcs are shown in Figure 3. The peripheral aryl groups are oriented essentially perpendicularly to the 4*N* mean plane, suggesting the existence of only a weak electronic interaction between the substituent aryl groups and the Pc core. The small difference in the position of the Q_{00} bands between **3a** (809 nm) and **3d** (824 nm) (or **3c**, 835; and **3e**, 844 nm) also supports the assumption that the aryl substitution effect is relatively weak (Supporting Information Figure S2). The distance between two chalcogenyl atoms of adjacently oriented isoindoles is close to twice the van der Waals radius of the corresponding elements, so that all Pcs exhibit a saddle-type distortion from the 4*N* mean plane, caused by the large substituents at the α-positions. Figure 4 shows the displacement of the 24 core atoms from the 4*N* mean plane, where the relationship between the size of the chalcogenyl atom and distortion of the Pc is clearly revealed. The degree of distortion of the core (Δr), which was calculated as the square root of the sum of square of the deviation of each atom from the mean plane, rationalizes the nonplanarity of the Pcs, as shown in the following order: **3d** (S, Δr = 0.27) < **3b** (Se, 0.41) < **3e** (Te, 0.61). In particular, **3e** has a more distorted structure than the previously reported nonplanar α-phenylated Pc (Δr = 0.58),[16] which is the most distorted Pc reported to date. Thus, the introduction of a large element at the α-position produces a highly enhanced saddle-like distortion.

2. Effect of Electron-Deficient Group 15 Elements in the Core. *Synthesis.* The preparation of group 15 element complexes containing sulfur atoms at the α-position is shown in Scheme 3. Phosphorus(V) complexes were synthesized according to the previously reported procedure[10] except for

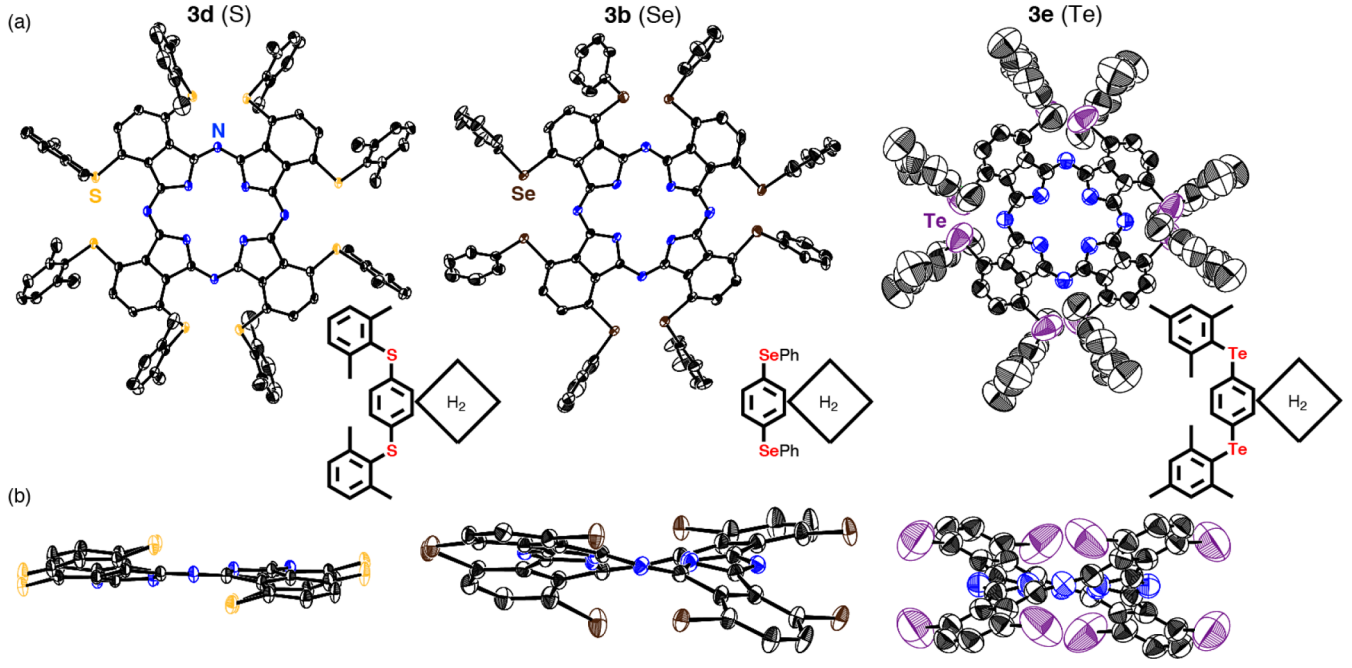

Figure 3. X-ray crystal structures of **3b**, **3d**, and **3e**. The thermal ellipsoids were scaled to the 50% probability level. (a) Top view; (b) side view (peripheral substituents omitted). H atoms and the solvent molecule have been omitted for clarity.

dx.doi.org/10.1021/ja411016f | J. Am. Chem. Soc. 2014, 136, 765−776

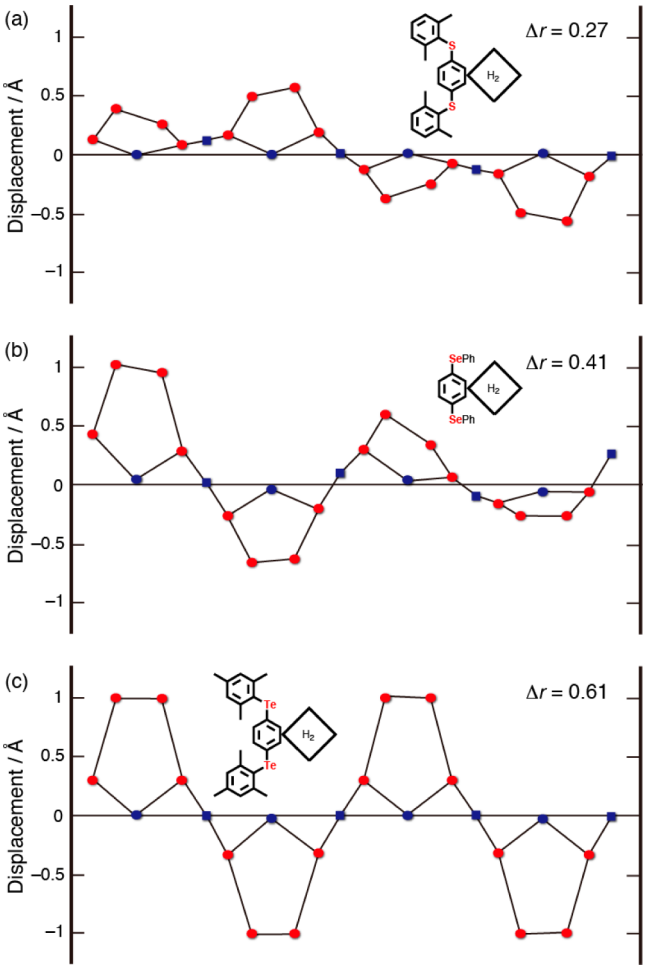

Figure 4. Views of the skeletal deviation of the atoms from the 4*N* mean plane for (a) **3d**, (b) **3b**, and (c) **3e**. Red ● indicate carbon atoms. Blue ■ and ● indicate nitrogen atoms at *meso*-positions and coordinating nitrogen atoms, respectively.

Scheme 3. Synthesis of Pc Complexes with Group 15 Elements[a]

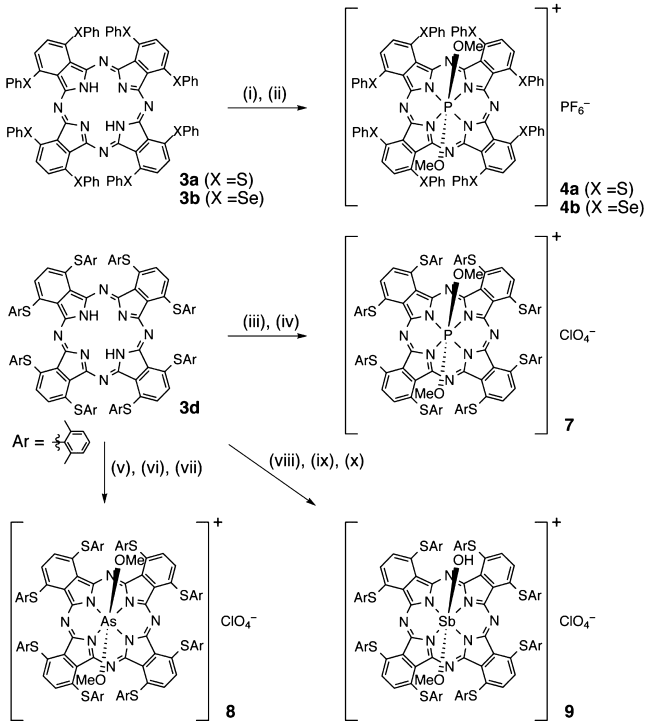

[a]Reagents and conditions: (i) $POBr_3$ (excess), pyridine, room temperature, 30 min (for **3a**) or reflux, 30 min (for **3b**); (ii) $MeOH/CH_2Cl_2$, room temperature, 30 min, then KPF_6 (excess), room temperature, 12 h, 85% (for **4a**), 46% (for **4b**); (iii) $POBr_3$ (excess), pyridine, room temperature, 4 h; (iv) $MeOH/CH_2Cl_2$, room temperature, 1 h, then $NaClO_4$ (excess), room temperature, 12 h, 85%; (v) $AsCl_3$ (excess), 2,6-lutidine/CH_2Cl_2, room temperature, 12 h; (vi) $HPyBr_3$ (1.5 equiv), room temperature, 1 h; (vii) $MeOH/CH_2Cl_2$, room temperature, 1 h, then $NaClO_4$ (excess), room temperature, 12 h, 30%; (viii) $SbBr_3$ (excess), 2,6-lutidine/CH_2Cl_2, room temperature, 1 h; (ix) Br_2 (2 equiv), room temperature, 90 min; (x) $NaClO_4$ (excess), $MeOH/CH_2Cl_2$, reflux, 12 h, 7%.

the reaction temperature. Here, the introduction of the P(V) ion proceeded at room temperature rather than at reflux temperature. It was considered that electron-rich group 16 elements on the Pc periphery can stabilize the electron-deficient P(V) complex by increasing the bond order between the pyrrole nitrogen and P(V) ion. The P(V) complexes of α-$(PhSe)_8$Pc and β-$(4\text{-}t\text{-}Bu\text{-}PhS)_8$Pc were similarly synthesized. Because α-chalcogenyl Pcs are thus suitable ligands for inserting group 15 elements into the central core, we next introduced As(V) and Sb(V) ions into the core of free-base α-thioaryl Pcs, although the previously reported As(V)[14] and Sb(V)[13] complexes were synthesized by a template method. In the case of the As(V) complex, $AsCl_3$ was utilized as the source of arsenic, and the production of an unstable As(III) complex was confirmed from the color change of the solution. Next, pyridinium tribromide was added to oxidize the As(III) ion to As(V),[17] followed by the introduction of axial ligands and the exchange of the counteranion. Finally, the desired As(V) complex **8** was isolated as an air-stable solid and characterized by ^{1}H NMR and HR-MALDI-FT-ICR-MS spectroscopy. The Sb(V) complex was similarly synthesized using $SbBr_3$ as the source of antimony. Although the $[(Pc)Sb(OMe)_2]^+X^-$ complex was relatively unstable in solution, a similar complex in which one axial OMe ligand was replaced by hydroxyl group was isolated by the method reported for porphyin Sb(V) complexes.[18]

Exceptional Red-Shift of the Q-Band by the Insertion of Phosphorus. Figure 5a shows the absorption spectra of several metal and phosphorus complexes of tetra *tert*-butylated Pc substituted at the β-position (β-^{t}Bu$_4$Pc, **10**) and α-$(PhS)_8$Pc. β-^{t}Bu$_4$Pc has usually been considered as a model of unsubstituted Pc, which is quite insoluble in organic solvents (the shift due to the introduction of four *tert*-butyl groups is small, ca. 6 nm).[19] As seen, the positions of the Q-band depend on the central element, but the difference is generally small (see data on Ni, Zn, Cu complexes). The manganese(III) complex is empirically known to be an exception, in that its Q-band appears in the longer wavelength region as compared to other metals and manganese(II) complexes.[20] On the other hand, when electron-donating groups such as PhS are introduced into the so-called α-positions, the shift is large, as typically seen in Figure 5a (bottom) on PhS substitution at the α-position. Here, the Q-band of free-base,[21] Mn, Ni, Cu, and Zn complexes shifts from ca. 670−680 nm for tetra β-^{t}Bu$_4$Pcs to ca. 790−810 nm for α-$(PhS)_8$Pcs (ca. 2300 cm^{-1} shift). As previously collected experimental data substantiate,[3] the Q-bands shift to the red through the substitution of electron-donating PhS groups even

dx.doi.org/10.1021/ja411016f | J. Am. Chem. Soc. 2014, 136, 765−776

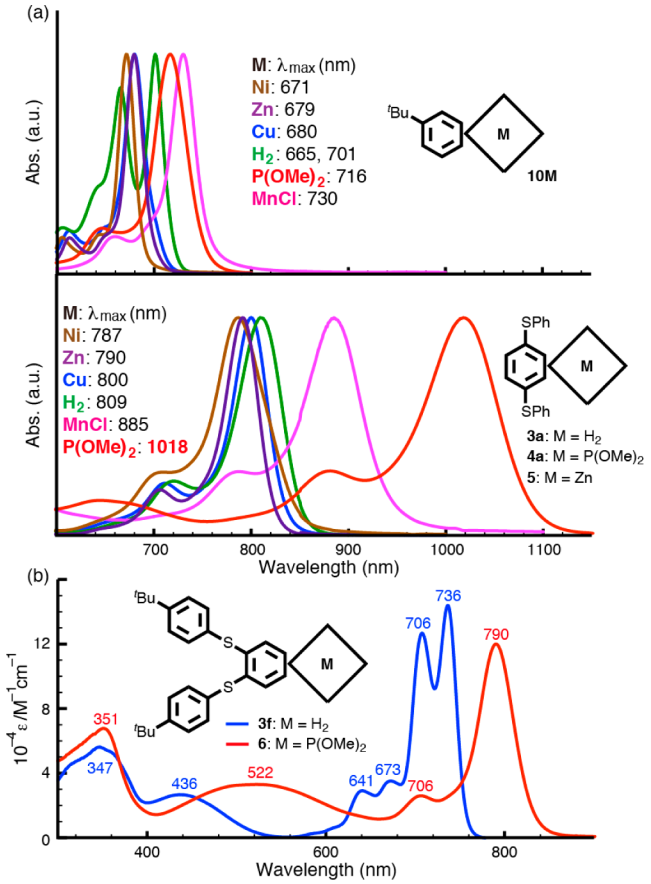

Figure 5. (a) Absorption spectra of metalated and phosphorus(V) complexes of β-^{t}Bu$_4$Pc (top) and those of α-(PhS)$_8$Pc (bottom) in $CHCl_3$. (b) Absorption spectra of free-base β-(thioaryl)$_8$Pc **3f** (blue) and β-(thioaryl)$_8$PcP(OMe)$_2$, that is, **6** (red) in $CHCl_3$. In (a), the intensity was normalized at the Q-band.

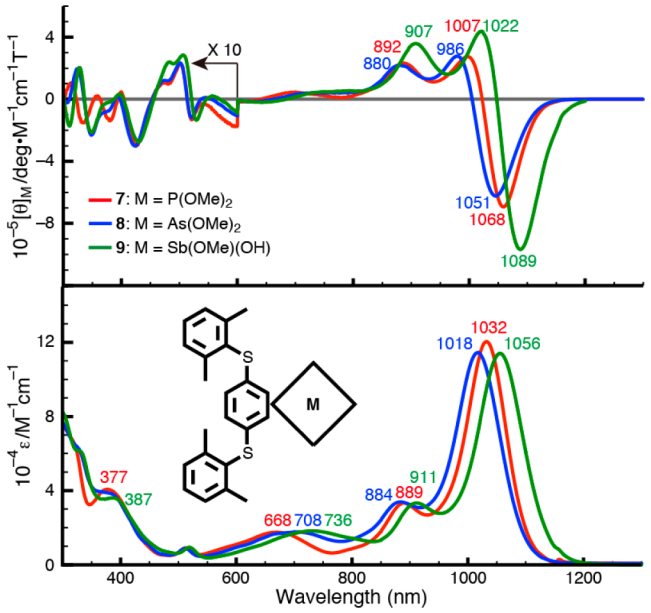

Figure 6. UV−vis−NIR absorption (bottom) and MCD (top) spectra of **7** (red), **8** (blue), and **9** (green) in CH_2Cl_2.

at the β-positions, although the extent is lower. Hence, for the transition metal (Mn, Ni, Cu, and Zn) complexes, the position of the Q-band is roughly predictable from the data of β-^{t}Bu$_4$Pcs, because the shift by metal insertion is not large. Interestingly, the Q-band of the phosphorus(V) complex **4a** having PhS groups at the α-positions was detected further to the red at 1018 nm. Thus, the insertion of phosphorus(V) ion yields a red-shift of ca. 210 nm (ca. 2500 cm^{-1}), while the difference between the β-^{t}Bu$_4$PcH$_2$ (**10H$_2$**) and β-^{t}Bu$_4$PcP(OMe)$_2$ (**10P**) is only ca. 30 nm (ca. 670 cm^{-1}).

To examine the dependence of the position of the substituents in P(V) complexes, the absorption spectra of free-base **3f** and its P(V) complex **6** were compared (Figure 5b). In **3f** and **6**, eight thioaryl groups were introduced at the β-positions of the Pc. The Q-band of **3f** (ca. 721 nm) is at shorter wavelength (by ca. 90 nm, ca. 1500 cm^{-1}) than that of the α-substituted free-base **3a** (809 nm), as we previously reported.[22] With the introduction of the P(V) ion to **3f**, the Q-band was shifted to 790 nm, but the difference (ca. 70 nm, ca. 1200 cm^{-1}) was smaller than that between **3a** and **4a** where eight PhS substituents were introduced at the α-positions. Therefore, it can be concluded that the position of the substituent groups is also a crucial factor in shifting the Q-band to the red beyond 1000 nm.

Optical Properties of Group 15 Complexes. The absorption and MCD spectra of group 15 complexes **7** (P), **8** (As), and **9** (Sb) are shown in Figure 6. The spectra of the other P(V) complexes with analogous substituents (**4a** and **4b**) are similar (Supporting Information Figure S3), and thus compounds **7**−**9** with the same substituents were chosen. P, As, and Sb have a similar electronegativity, so that the effect of these elements on the electronic structure is inferred to be similar. The Q-band of all of the complexes appears in the deep near-IR region, beyond 1000 nm (1032 nm for **7**, 1018 nm for **8**, and 1056 nm for **9**), with intense (ε: 1.20 × 10^5 M^{-1} cm^{-1} for **7**, 1.15 × 10^5 M^{-1} cm^{-1} for **8**, 1.14 × 10^5 M^{-1} cm^{-1} for **9**) and sharp (fwhm: 780 cm^{-1} for **7**, 890 cm^{-1} for **8**, 850 cm^{-1} for **9**) bands in CH_2Cl_2. The intense Faraday *A*-term MCD spectra in the Q-band region further indicate that the practical chromophore symmetry of **7**−**9** is close to D_{4h}, similar to regular metalated Pcs. These results suggest that the electronic structures of **7**−**9** are similar to those of the typical Pcs, although the Q-bands appear at much longer wavelength beyond 1000 nm.

To date, some Pcs have been known as good fluorophores[23] due to their rigid structures, while the development of organic dyes having emission beyond 1000 nm has been quite challenging, and this type of molecule has been quite limited.[24] To have emission beyond 1000 nm, in principle, chromophores must have an intense absorption band near 1000 nm, but these chromophores are difficult to prepare. In addition, even if they have strong, allowed absorption in this region, these molecules generally do not show emission, due to the small energy gap between the ground and excited states. Our molecules **7**−**9** at least have intense absorption bands beyond 1000 nm, and their optical properties appear similar to those of normal Pcs. Thus, we measured the emission spectra of these molecules (Figure 7). Commercially available polymethine dye IR-1048 was used as a standard for the fluorescence quantum yield (λ_{max} = 1058 nm and Φ_{FL} = 4 × 10^{-3} in CH_2Cl_2).[24c] Compounds **7** and **8** showed a distinct fluorescence beyond 1000 nm with relatively high quantum yields (Φ_{FL} = 6 × 10^{-3} and 7 × 10^{-3}, respectively), while a weaker emission was observed in **9** (Φ_{FL} = 2 × 10^{-3}), possibly due to the heavy atom effect of the antimony atom. The Stokes shifts were small (430−500 cm^{-1}), as expected from the emission spectrum of typical rigid

dx.doi.org/10.1021/ja411016f | J. Am. Chem. Soc. 2014, 136, 765−776

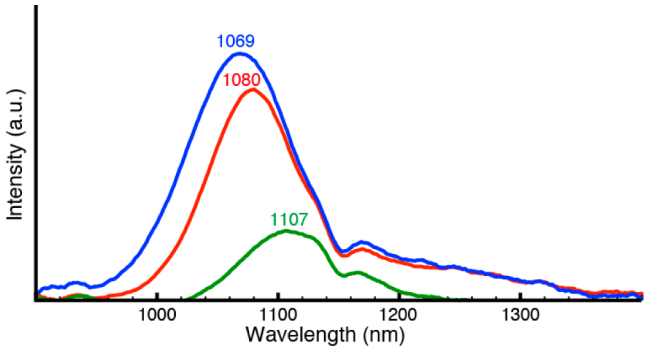

Figure 7. Emission spectra excited at 880 nm of **7** (red), **8** (blue), and **9** (green) in CH_2Cl_2 in the near-IR region.

metalated Pcs, supporting the origin of the fluorescence in **7**–**9** is the Pc macrocycle.

Despite the intense Q-band in the near-IR region, the group 15 complexes of Pcs can be stored as solids under ambient conditions for over 6 months. In general, the photostability of zinc Pc complexes is usually low due to a singlet oxygen-mediated photobleaching process.[25] Copper complexes of Pcs are, however, stable, and their robustness can be applied in various fields. Accordingly, to estimate the photostability of the complexes in this study, changes in optical density at the peak absorption maxima of IR-1048, copper, zinc (**5**), and phosphorus (**4a** and **4b**) complexes were measured in $CHCl_3$ under ambient light (Supporting Information Figure S4). Here, the Pc complexes are substituted with either eight PhS (copper, zinc (**5**), and **4a**) or eight PhSe (**4b**) groups at the α-positions. The decrease in intensity of the Q-band of **4a** was greater than the corresponding copper complex, but less than IR-1048, having moderate fluorescence in the same region. Thus, when approximately 10^{-6} M of the solution was irradiated under the same conditions, the copper complex, **4a**, IR-1048, and **4b** were decomposed completely after ca. 160, 130, 90, and 40 h, respectively, while the zinc complex **5** decomposed in only 3 h. Such a high photostability seen for **4a**, exceeding the commercially available near-IR fluorescence dye IR-1048, is unusual and fairly remarkable. This can be explained by the low-lying HOMO and small HOMO–LUMO band gap of **4a** (see sections on Electrochemistry and Molecular Orbital Calculations). On the other hand, the stability of selenium-substituted **4b** with a Q-band peak at 1033 nm is lower than that of **4a** with a Q-band peak at 1018 nm. A possible reason for this may be the heavy atom effect of selenium.

Solid-State Structures of Group 15 Complexes. Except for the antimony complexes of Pcs,[13d] the solid-state structures of group 15 complex of Pcs have been virtually unexplored. The crystallographic structure of the As(III) complex of Pc was reported but investigated only in the solid state.[12] No crystallographic structures of phosphorus complexes of Pc had been reported before our previous communication.[10] In this work, the first X-ray crystallographic analysis of an As(V) complex of Pc (**8**) having eight ArS groups at the α-positions has been achieved from a single crystal, which was obtained by slow diffusion of *n*-hexane into a solution of **8** in CH_2Cl_2. Single crystals suitable for X-ray analysis of the zinc complex of α-$(PhS)_8Pc$ (**5**) were also obtained. Crystallographic structures of phosphorus (**4a**), zinc (**5**), and arsenic (**8**) complexes of α-$(ArS)_8Pc$ are shown in Figure 8, and the structural deviations from the 4*N* mean plane of the Pc macrocycles are summarized in Figure 9. The structure of As(V) complex **8** was first determined unambiguously. The arsenic ion sits in the center of the 4*N* Pc mean plane ($\Delta 4N < 0.005$ Å), and the macrocycle is highly planar ($\Delta r = 0.05$), while the structure of the P(V) complex is severely ruffled ($\Delta r = 0.43$). The difference in the structures between P(V) and As(V) complexes with similar absorption properties may be at least partly explained by the differences in the physical properties of phosphorus and arsenic elements. According to the periodic table, the atomic radius of arsenic (120 pm) is larger than that of phosphorus (106 pm)

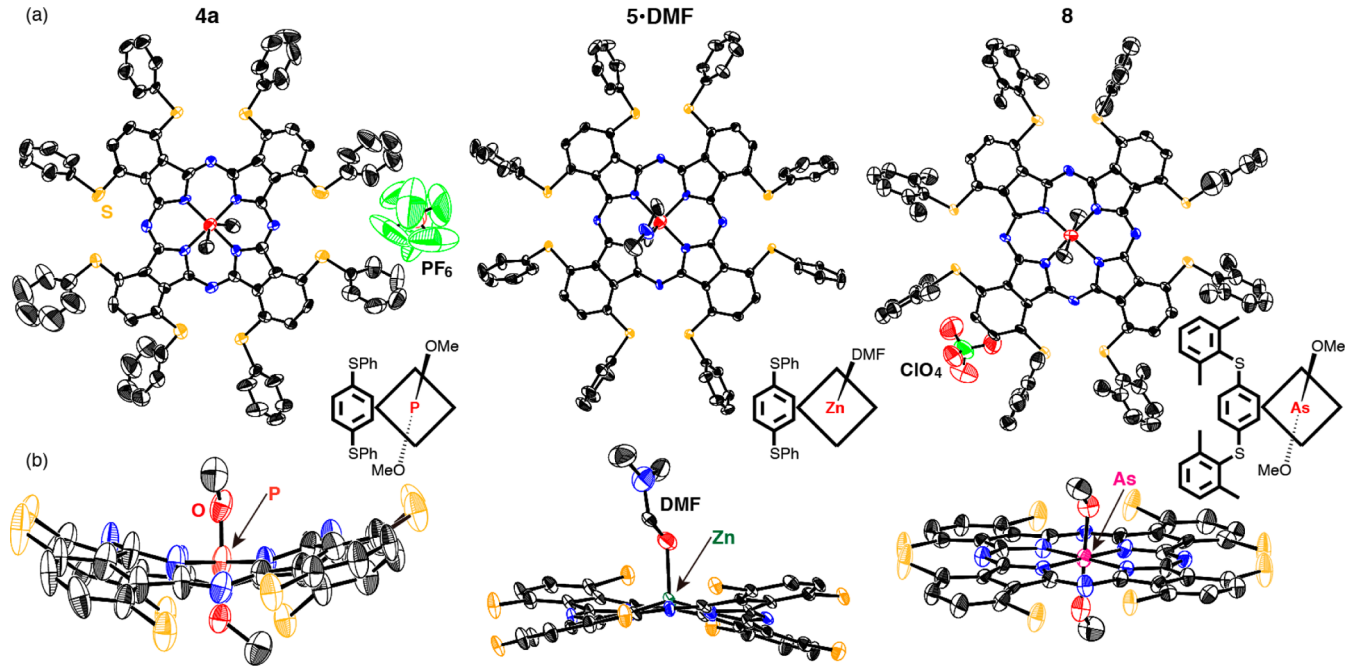

Figure 8. X-ray crystal structure of **4a**, **5·DMF**, and **8**. The thermal ellipsoids were scaled to the 50% probability level. (a) Top view; (b) side view (peripheral substituents omitted). H atoms, the counteranion of **4a** and **8**, and the solvent molecule have been omitted for clarity.

dx.doi.org/10.1021/ja411016f | J. Am. Chem. Soc. 2014, 136, 765–776

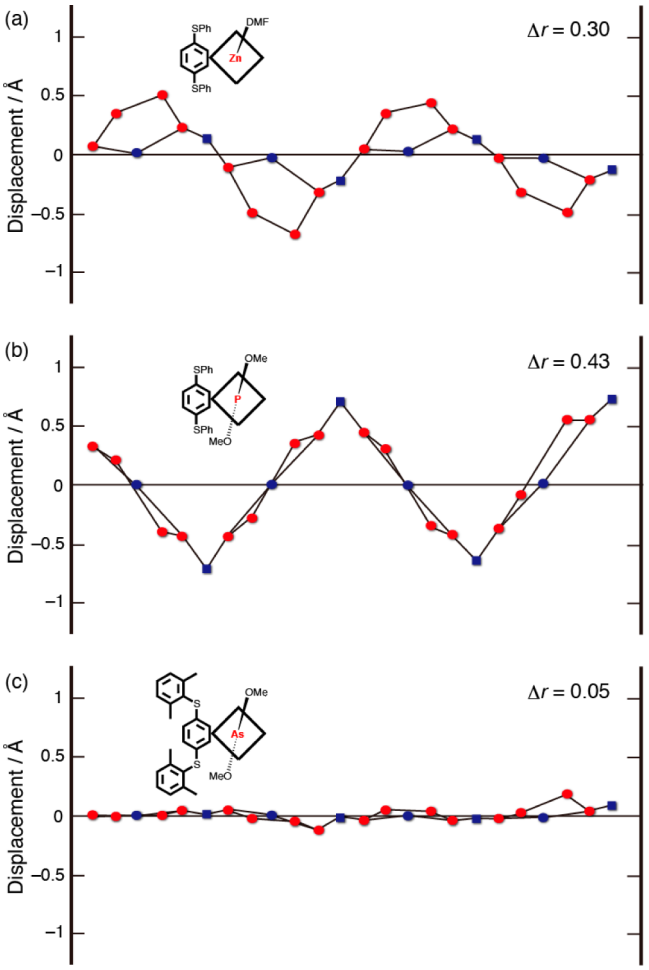

Figure 9. Views of the skeletal deviation of the atoms from the 4*N* mean plane for (a) **5·DMF**, (b) **4a**, and (c) **8**. Red ● indicate carbon atoms. Blue ■ and ● indicate nitrogen atoms at *meso*-positions and coordinating nitrogen atoms, respectively.

and appears to be just the right size to fit into the center of the Pc ligand, so that arsenic only marginally affects the structure of the macrocycle, while phosphorus(V) is particularly small so that the Pc ligand has to deform or shrink to coordinate to it. The structure of **8** containing $As(OMe)_2$ in the solid state was more planar than that of the corresponding free-base Pc **3d**, but this may be due to the difference of packing structure. In the molecular-packing diagram of **8**, the Pc molecules are arrayed in a π-slipped-stack form (Supporting Information Figure S5).

The crystallographic structure of **5** was obtained as one DMF molecule coordinated at the axial position of the zinc ion (**5·DMF**). The central zinc ion is deviated by 0.42 Å from the 4*N* mean plane due to the axial coordination, similarly to previously reported pentacoordinated zinc Pc.[26] The Δr of **5·DMF** (0.30) is similar to that of the corresponding free-base **3d**, indicating that the zinc ion does not significantly affect the structure of the macrocycle and that the origin of the structural ruffling of **4a** may be the phosphorus(V). If we compare the distance between the two pyrrole-nitrogen atoms at opposite sides in the core, it is 3.67 Å for **4a**, and this value is smaller than those of **5·DMF** (3.96 Å) and the other free-base Pcs (4.01−3.84 Å) in this study. The bond length between phosphorus and nitrogen in the core of **4a** is 1.84 Å, which is reasonable for a single bond of hexacoordinated phosphorus(V)−nitrogen.[27] Therefore, after insertion of phosphorus into the center of the Pc, the phosphorus atom seems to attract the pyrrole−nitrogen to give a short bond length, producing the severely ruffled Pcs.

Electrochemistry. It is well established that the HOMO and LUMO energies of Pc derivatives correlate well with their first oxidation and reduction potentials.[28] Estimating the values of redox potentials is also important to determine the origins of the red-shift of the Q-band wavelength accompanying the introduction of main group elements. Figure 10 displays cyclic

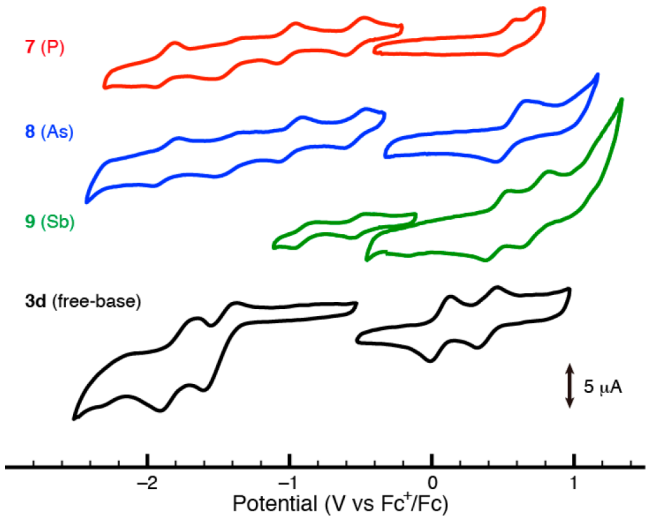

Figure 10. Cyclic voltammetry data for **3d** and **7**−**9**. Cyclic voltammograms were acquired from 1.0 mM solutions of analyte in 0.1 M ^{n}Bu$_4$NClO$_4$/*o*-DCB. Ferrocene was used as an internal standard and set to 0 V.

voltammograms of free-base **3d**, and its group 15 complexes (central ion = **7** (P(V)(OMe)$_2$), **8** (As(V)(OMe)$_2$), and **9** (Sb(V)(OH)(OMe)) in *o*-dichlorobenzene (DCB) with 0.1 M ^{n}Bu$_4$NClO$_4$ as the supporting electrolyte. The redox potential data are summarized in Table 1. **3d** showed couples at 0.39, 0.06, −1.45, and −1.78, and the gap between the first redox potentials ($E_{1ox} - E_{1red}$ = 1.51 V) was smaller than that of β-^{t}Bu$_4$PcH$_2$ ($E_{1ox} - E_{1red}$ = 1.70 V) obtained under the same conditions as previously reported.[5a] In the case of **7**−**9**, both of the redox potentials are shifted anodically, and small gaps (1.07, 1.10, and 0.96 V for **7**, **8**, and **9**, respectively) are observed, in good agreement with the positions of the Q-bands in absorption spectra (1032, 1018, and 1056 nm in the order of **7**, **8**, and **9**, respectively, derived from Figure 6). In particular, the change in reduction potential is larger than that of oxidation potential. These redox potential data indicate that, although both the HOMO and the LUMO stabilize on insertion of a group 15 element into the Pc core, the stabilization of the LUMO is larger than that of the HOMO. Therefore, the origin

Table 1. Redox Potential (V) Data (vs Fc$^+$/Fc) for 3d and 7−9

	E_{red4}	E_{red3}	E_{red2}	E_{red1}	E_{ox1}	E_{ox2}	ΔE^a
3d			−1.78	−1.45	0.06	0.39	1.51
7	−1.86	−1.43	−1.02	−0.54	0.53		1.07
8	−1.87	−1.42	−0.99	−0.54	0.56		1.10
9			−0.95	−0.49	0.47	0.72	0.96

$^a\Delta E$ (V) indicates the potential differences between E_{ox1} and E_{red1}.

dx.doi.org/10.1021/ja411016f | J. Am. Chem. Soc. 2014, 136, 765−776

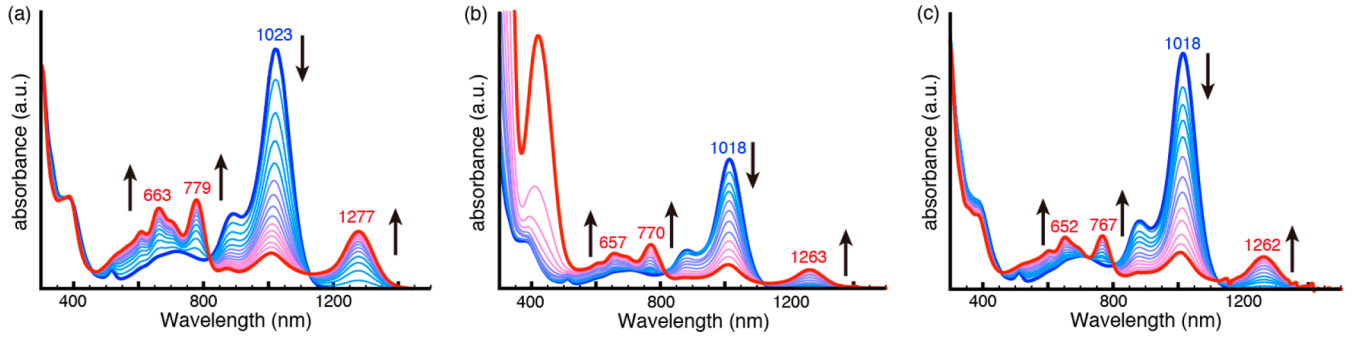

Figure 11. Spectral changes of **8** solution by (a) applying −0.2 V potential vs Ag/AgCl reference electrode in *o*-DCB, (b) adding $Me_{10}Fc$ in CH_2Cl_2, and (c) adding triethylamine in CH_2Cl_2.

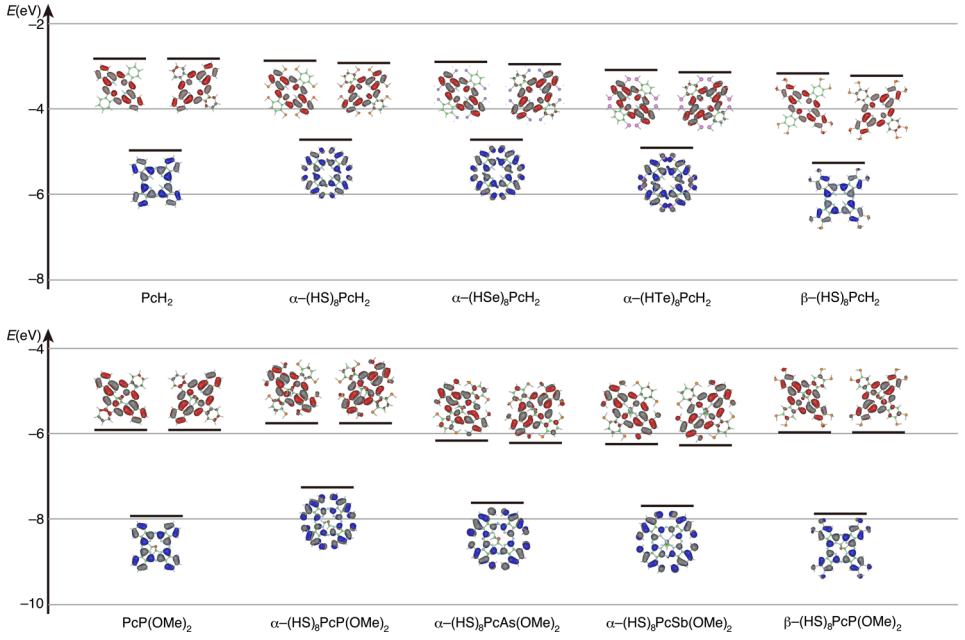

Figure 12. Energy levels of frontier MOs and their contour plots obtained from calculations. Blue and red plots indicate occupied and unoccupied MOs, respectively. Calculations were performed at the B3LYP/6-31G* level (for details, see the Supporting Information).

of the red-shift of the Q-band after the insertion of the group 15 element is due to some anodic shift of the first oxidation potential and a significant anodic shift of the first reduction potential. This shows a good contrast to the reduction of the gap of the first redox potentials ($E_{1ox} - E_{1red}$) observed on going from tetraazaporphyrin to Pc, naphthalocyanine, and anthracocyanine. Here, on ring expansion by benzoannulation, the first oxidation potential shifts significantly cathodically, while the first reduction potential remains almost the same or shifts only slightly cathodically.[4a]

The group 15 complexes exhibit high stability under oxidative conditions and, from the above electrochemistry data, can be good electron acceptors. For assignment of the reduced species, spectroelectrochemical measurements were performed, with representative results for As(V) complex **8** shown in Figure 11a. When a potential negative enough for the first reduction to occur was applied, the Q-band of **8** was diminished, and new medium-intensity bands appeared in the deep near-IR region (1277 nm) and the visible to near-IR regions (779 and 663 nm) accompanying a set of sharp isosbestic points. The final absorption spectrum is characteristic of a one-electron reduced Pc ligand,[29] indicating that the reduction of the Pc ligand is easier than that of the electron-deficient arsenic ion. The original spectrum of **8** was restored upon application of anodic potentials or without applying any potential, confirming the reversibility of the first reduction process. On the basis of **8**'s stability during the first reduction, chemical doping of **8** was next examined. For example, as a reductant, increasing amounts of decamethylferrocene ($Me_{10}Fc$, $E^{\circ\prime}$ = −0.59 V vs Fc^+/Fc in CH_2Cl_2[30]) were added to the CH_2Cl_2 solution of **8**, and the spectroscopic change shown in Figure 11b was observed, which is essentially similar to that shown in Figure 11a during electrochemical reduction. An analogous spectroscopic change was also effected by the addition of a weak Lewis base. Here, after adding excess triethylamine to a CH_2Cl_2 solution of **8**, the resultant spectrum fully matched both of the spectra of electronically and chemically reduced species (Figure 11c). Moreover, the base-doped intermediate could be neutralized with excess trifluoroacetic acid, to restore the original spectrum of **8**. These spectral changes of **8** in the deep near-IR region could be repeated several times by adding triethylamine and trifluoroacetic acid alternately, illustrating good reversibility between the species.

3. Molecular Orbital Calculations. Molecular orbital (MO) calculations were performed for unsubstituted H_2Pc and Pcs containing group 15 and 16 elements as models of the

dx.doi.org/10.1021/ja411016f | J. Am. Chem. Soc. 2014, 136, 765−776

Table 2. Calculated Excited Wavelength (λ) and Oscillator Strengths (f) for the Components of Q-Bands

compound	$\Delta(E_{LUMO}-E_{HOMO})$ (eV)	λ (nm)	f	composition (%)[a]
PcH_2	2.15	600.4	0.39	H→L+1 (71%), H−1→L (6%)
		593.7	0.44	H→L (71%), H−1→L+1 (3%)
α-$(HS)_8PcH_2$	1.82	726.0	0.42	H→L (74%)
		724.5	0.35	H→L+1 (75%)
α-$(HSe)_8PcH_2$	1.79	755.4	0.30	H→L+1 (75%)
		754.9	0.38	H→L (74%)
α-$(HTe)_8PcH_2$	1.78	765.6	0.34	H→L (96%)
		760.6	0.27	H→L+1 (93%)
β-$(HS)_8PcH_2$	2.07	629.3	0.49	H→L (92%)
		624.9	0.56	H→L+1 (95%)
$PcP(OMe)_2$	2.02	648.9	0.32	H→L (96%)
		647.7	0.32	H→L+1 (96%)
α-$(HS)_8PcP(OMe)_2$	1.51	915.8	0.26	H→L (97%), H−1→L (3%)
		913.0	0.26	H→L+1 (97%), H−1→L+1 (3%)
α-$(HS)_8PcAs(OMe)_2$	1.43	990.5	0.18	H→L (85%), H→L+1 (8%)
		911.8	0.29	H→L+1 (86%), H→L (9%)
α-$(HS)_8PcSb(OMe)_2$	1.41	987.7	0.19	H→L (92%), H−1→L (8%)
		940.7	0.26	H→L+1 (93%), H−1→L+1 (7%)
β-$(HS)_8PcP(OMe)_2$	1.89	712.0	0.30	H→L (83%), H→L+1 (8%)
		709.6	0.31	H→L+1 (82%), H→L (8%)

[a]H−1, H, L, and L+1 denote HOMO−1, HOMO, LUMO, and LUMO+1, respectively.

Table 3. MO Energies (eV) and the Energy Difference Predicted in the TD-DFT Calculations, Together with Experimental ΔHL Derived from Absorption Spectra

compound	HOMO	LUMO	LUMO+1	$\Delta(E_{LUMO}-E_{HOMO})_{calcd}$	Q_{exp} (nm)[a]	$\Delta(E_{LUMO}-E_{HOMO})_{exp}$
PcH_2	−4.95	−2.80	−2.78	2.15	683 (**10H$_2$**)	1.82
$PcP(OMe)_2$	−7.95	−5.93	−5.92	2.02	716 (**10P**)	1.73
α-$(HS)_8PcH_2$	−4.71	−2.88	−2.83	1.83	809 (**3a**)	1.53
α-$(HS)_8PcP(OMe)_2$	−7.26	−5.75	−5.74	1.51	1018 (**4a**)	1.22
β-$(HS)_8PcH_2$	−5.27	−3.20	−3.15	2.07	721 (**3f**)	1.72
β-$(HS)_8PcP(OMe)_2$	−7.88	−5.99	−5.98	1.89	790 (**6**)	1.57

[a]The value was derived from a compound written in parentheses. The absorption spectrum was measured in $CHCl_3$ solution.

synthesized Pcs in this study. Model structures whose substituents on the group 16 elements were replaced by hydrogen were used because these groups affect the absorption spectra only marginally. Partial MOs related to the Q-band absorptions are shown in Figure 12, with calculated transition energies, oscillator strengths (f), and configurations summarized in Table 2. The optimized structures of α-$(HS)_8PcH_2$, α-$(HSe)_8PcH_2$, and α-$(HTe)_8PcH_2$ are also distorted, the distortion becoming larger on going from α-$(HS)_8PcH_2$ (Δr = 0.36) to α-$(HTe)_8PcH_2$ (Δr = 0.57), in good agreement with the crystal structures of α-chalcogenyl Pcs (Figure 3). As has already been reported for sulfur,[22] the introduction of group 16 elements into the α-position can destabilize the HOMO almost selectively so that the HOMO−LUMO gap ($\Delta(E_{LUMO}-E_{HOMO})$) becomes smaller. The introduction of group 15 elements into the center of the Pc stabilizes both the HOMO and the LUMO significantly (the extent for the LUMO is higher). The difference among group 15 elements is relatively small, and the estimated $\Delta(E_{LUMO}-E_{HOMO})$ values for $[\alpha$-$(HS)_8PcX(OMe)_2]^+$ (X = P, As, Sb) are smaller (1.4−1.5 eV) as compared to those without group 15 elements (ca. 1.8 eV, Table 2). The origin of the narrow band gap may be attributable to the greater stabilization of the LUMO (ca. 3.5 eV) than that of the HOMO (ca. 2.9 eV), as indeed is suggested from the experimental redox potentials (Table 1). In the case of antimony, α-$(HS)_8PcSb(OMe)$ with Sb(III) oxidation state was also calculated, because both Sb(III) and Sb(V) were isolated and reported previously[13b] (Supporting Information Figure S6). The calculated $\Delta(E_{LUMO}-E_{HOMO})$ value (1.55 eV) of the Sb(III) complex is larger than that of the Sb(V) complex (1.41 eV), in accordance with the relative Q-band positions of the Sb(III) intermediate (974 nm in CH_2Cl_2) and Sb(V) species in this study (1056 nm) (Supporting Information Figure S7). Even after the introduction of both group 15 and 16 elements, the envelopes of the frontier orbitals of the Pc ligand are similar to those of unsubstituted Pcs, and the calculated transitions in the Q-band region are composed of the HOMO, LUMO, and LUMO+1. These orbitals derived from Gouterman's "four-orbital" theory[31] indicate that these absorption bands can be explained in a manner similar to that of typical free-base or metalated Pcs. Therefore, it may be concluded that the π-conjugation of these near-IR absorbing Pcs in this study has not been markedly changed from that of normal Pcs, so that the enormous (~400 nm from PcH_2) red-shift of the Q-band could be achieved as a result of pure substitution effects.

To enhance the interpretation of the effect with respect to the Pc ligand, position of group 16 elements, and central group 15 element in this study, the results of MO calculations of some free-base and P(V) complexes were compared. The calculated values of frontier MO energy, potential differences calculated therefrom ($\Delta(E_{LUMO}-E_{HOMO})_{calcd}$), and the experimental

dx.doi.org/10.1021/ja411016f | J. Am. Chem. Soc. 2014, 136, 765−776

Table 4. Predicted HOMO, LUMO, and ΔHL Change (eV) on Going from One Species to Another (ΔHOMO, ΔLUMO, and $\Delta(\Delta(E_{LUMO}-E_{HOMO}))$, Respectively), Together with Experimental $\Delta(\Delta(E_{LUMO}-E_{HOMO}))$[a]

	ΔHOMO	ΔLUMO	$\lvert\Delta(\Delta(E_{LUMO}-E_{HOMO}))\rvert$	$\lvert\Delta(\Delta(E_{LUMO}-E_{HOMO}))_{exp}\rvert$
$PcH_2 \rightarrow PcP(OMe)_2$	−3.00	−3.13	0.13	0.08
$PcH_2 \rightarrow \alpha\text{-}(HS)_8PcH_2$	0.24	−0.08	0.32	0.35
$PcH_2 \rightarrow \beta\text{-}(HS)_8PcH_2$	−0.32	−0.40	0.08	0.10
$PcH_2 \rightarrow \alpha\text{-}(HS)_8PcP(OMe)_2$	−2.31	−2.95	0.64	0.60
$PcH_2 \rightarrow \beta\text{-}(HS)_8PcP(OMe)_2$	−2.93	−3.19	0.26	0.25
$\alpha\text{-}(HS)_8PcH_2 \rightarrow \alpha\text{-}(HS)_8PcP(OMe)_2$	−2.55	−2.87	0.32	0.32
$\beta\text{-}(HS)_8PcH_2 \rightarrow \beta\text{-}(HS)_8PcP(OMe)_2$	−2.61	−2.79	0.18	0.15

[a]Calculated data are derived from data in Table 3, and experimental $\Delta(\Delta(E_{LUMO}-E_{HOMO}))$ corresponds to the Q-band shift.

potential differences derived from their absorption spectra ($\Delta(E_{LUMO}-E_{HOMO})_{exp}$) are summarized in Table 3. There is a clear correlation between $\Delta(E_{LUMO}-E_{HOMO})_{calcd}$ and the Q-band position, expressed in units of eV for the six representative compounds (Supporting Information Figure S8). Therefore, we can have a detailed discussion about the origin of the substitution effects using the calculated MO energies and differences between compounds in this study. Table 4 summarizes the energy differences of the frontier MO energy on going from one species to another. The following results may be extracted from these data. (1) A P(V) ion can stabilize both the HOMO and the LUMO, but the $\Delta(E_{LUMO}-E_{HOMO})$ depends on the position of the substituent. When a P(V) ion is introduced to unsubstituted Pc, the stabilization of the LUMO is larger (ΔLUMO value of −3.13 eV) than that of the HOMO (−3.00 eV), and once a sulfur atom is introduced at either eight α or eight β positions, the extent of the stabilization of the LUMO (−0.08 and −0.40 eV, for α- and β-substituted species, respectively) is also larger than that of the HOMO (0.24 and −0.32 eV). The energy gap ($\Delta(E_{LUMO}-E_{HOMO})_{calcd}$ = 1.51 eV) of $\alpha\text{-}(HS)_8PcP(OMe)_2$ is significantly smaller than those of other species, indicating that the introduction of electron-donating group 16 elements at the α-position is extraordinarily efficient, as is indeed substantiated experimentally (Figure 5a). (2) As seen on going from PcH_2 to $\alpha\text{-}(HS)_8PcH_2$, the introduction of HS groups at the α positions destabilizes the HOMO energy, so that the ΔHL value becomes significantly smaller ($\lvert\Delta(\Delta(E_{LUMO}-E_{HOMO}))\rvert$ = 0.32 eV), while, as anticipated, on going from PcH_2 to $\beta\text{-}(HS)_8PcH_2$, the substituent at the β-position stabilizes both the HOMO and the LUMO energy so that the decrease of ΔHL is very small ($\lvert\Delta(\Delta(E_{LUMO}-E_{HOMO}))\rvert$ = 0.08 eV). This indicates that the introduction of group 16 elements at the α-positions is indispensable in shifting the band markedly to the red. (3) When $P(OMe)_2$ is inserted into α- or $\beta\text{-}(HS)_8PcH_2$, the $\lvert\Delta(\Delta(E_{LUMO}-E_{HOMO}))\rvert$ is larger for $\alpha\text{-}(HS)_8PcH_2$ (0.32 eV) than for $\beta\text{-}(HS)_8PcH_2$ (0.18 eV), suggesting that the effect of phosphorus is larger when inserted into Pcs having group 16 elements at the α-positions. Thus, judging particularly from (2) and (3), the introduction of electron-donating group 16 elements at eight α-positions and insertion of a high valence group 15 element appears to be an effective strategy for shifting the Q-band to the red, also supported strongly by the results of MO calculations.

CONCLUSION

A series of near-IR absorbing Pcs containing group 15 elements in the center and group 16 elements as substituents have been synthesized in a few-steps reaction in moderate yields, and their structural and spectroscopic properties have been elucidated. In the first part, the structure and electronic properties of the free-base Pcs containing electron-donating group 16 elements as peripheral substituents were clarified. The position of the Q-band and the distortion of the Pc macrocycle appear to be correlated with the electronegativity and atomic radius of chalcogenyl elements. In particular, the crystallographic structure of $\alpha\text{-}(ArTe)_8PcH_2$ **3e** revealed that it is the most distorted simple free-base Pc ever reported.[32] In the second part, we examined the spectroscopic relationships between the type of Pc ligand and a central P(V) ion, where the extent of the red-shift upon phosphorus insertion was found to be different from ligand to ligand. Here, only the combination of peripheral group 16 elements at α-positions and a central P(V) ion was able to shift the Q-band beyond 1000 nm (Figure 13).

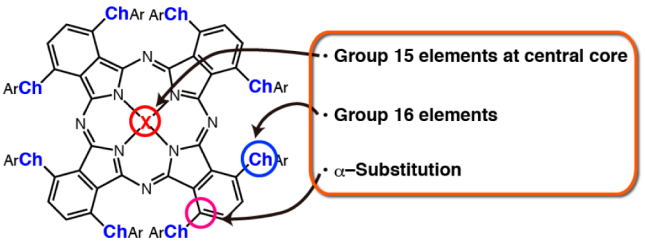

Figure 13. Criteria for Pcs absorbing in the near-IR region beyond 1000 nm.

The syntheses of As(V) and Sb(V) complexes were also achieved, and these complexes showed fluorescence in the 960−1400 nm region with moderate quantum yields. The first crystallographic structures of P(V) and As(V) complexes revealed that the structure of the Pc macrocycle could be controlled by the ionic size of the central element without changing the absorption properties.

Although all P(V), As(V), and Sb(V) Pcs in this study showed intense absorption peaks beyond 1000 nm, they had comparative stability to CuPc against light exposure due to their low-lying HOMO, which suggests the possibility of commercial practical applications. Reversible spectroscopic changes in the near-IR region were also observed upon addition of a weak Lewis base, reflecting that these Pcs can act as good electron acceptors. Cyclic voltammetric measurements revealed, while MO calculations predicted, that the marked red-shift on P(V) insertion is due to a decrease of the HOMO−LUMO gap, originating from significant stabilization of the LUMO and moderate stabilization of the HOMO. The extent of the Q-band shift on introducing a group 16 element at eight α- or β-positions and phosphorus insertion was predicted independently by MO calculations, and the magnitude of the total calculated shift agreed very well with the experiments

dx.doi.org/10.1021/ja411016f | J. Am. Chem. Soc. 2014, 136, 765−776

(Table 4). The substantial red-shift appears to originate from pure substitution effects, including central group 15 elements, peripheral group 16 elements, and positions of the latter. The Pcs in this study are easy to synthesize, robust, free from transition metals, and have predictable properties. The novel strategy reported here will open the door to practical applications of near-IR dyes beyond 1000 nm.

■ ASSOCIATED CONTENT

Supporting Information

Additional synthetic, spectroscopic, and calculation results, full details of experimental and calculation procedures, and X-ray crystallographic data (CIF). This material is available free of charge via the Internet at http://pubs.acs.org.

■ AUTHOR INFORMATION

Corresponding Author

nagaok@m.tohoku.ac.jp

Notes

The authors declare no competing financial interest.

■ ACKNOWLEDGMENTS

This work was partly supported by a Grant-in-Aid for Scientific Research on Innovative Areas (25109502, "Stimuli-responsive Chemical Species"), Scientific Research (B) (No. 23350095), Challenging Exploratory Resarch (No. 25620019), and Young Scientist (B) (No. 24750031) from the Ministry of Education, Culture, Sports, Science, and Technology (MEXT). We thank Prof. Takeaki Iwamoto, Dr. Shintaro Ishida, and Dr. Eunsang Kwon (Tohoku University) for X-ray measurements, Prof. Masanobu Uchiyama (The University of Tokyo and RIKEN), and Dr. Atsuya Muranaka (RIKEN) for near-IR MCD and fluorescence measurements. Some of the calculations were performed using supercomputing resources at the Cyberscience Center of Tohoku University.

■ REFERENCES

(1) *Functional Dyes*; Kim, S.-H., Ed.; Elsevier: Amsterdam, Netherlands, 2006.

(2) (a) *Handbook of Porphyrin Science*; Kadish, K. M., Smith, K. M., Guilard, R., Eds.; World Scientific Publishing: Singapore, 2010. (b) *The Porphyrin Handbook*; Kadish, K. M., Smith, K. M., Guilard, R., Eds.; Academic Press: San Diego, CA, 2003. (c) Mckeown, N. B. *Phthalocyanine Materials: Synthesis, Structure and Function*; Cambridge University Press: Cambridge, UK, 1998. (d) *Phthalocyanines: Properties and Applications*; Leznoff, C. C., Lever, A. B. P., Eds.; VCH: Weinheim, Germany, 1989. (e) Mack, J.; Kobayashi, N. *Chem. Rev.* **2011**, *111*, 281−321.

(3) Fukuda, T.; Kobayashi, N. In *Handbook of Porphyrin Science*; Kadish, K. M., Smith, K. M., Guilard, R., Eds.; World Scientific: Singapore, 2010; Vol. 9, pp 1−650.

(4) (a) Kobayashi, N.; Nakajima, S.; Ogata, H.; Fukuda, T. *Chem.-Eur. J.* **2004**, *10*, 6294−6312. (b) Yeung, Y.-O.; Liu, R. C. W.; Law, W.-F.; Lau, P.-L.; Jiang, J.; Ng, D. K. P. *Tetrahedron* **1997**, *53*, 9087−9096. (c) Freyer, W.; Stiel, H.; Teuchner, K.; Leupold, D. *J. Photochem. Photobiol., A* **1994**, *80*, 161−167. (d) Hanack, M.; Renz, G.; Straehle, J.; Schmid, S. *J. Org. Chem.* **1991**, *56*, 3501−3509. (e) Freyer, W.; Mueller, S.; Teuchner, K. *J. Photochem. Photobiol., A* **2004**, *163*, 231−240.

(5) (a) Furuyama, T.; Ogura, Y.; Yoza, K.; Kobayashi, N. *Angew. Chem., Int. Ed.* **2012**, *51*, 11110−11114. (b) Matsushita, O.; Derkacheva, V. M.; Muranaka, A.; Shimizu, S.; Uchiyama, M.; Luk'yanets, E. A.; Kobayashi, N. *J. Am. Chem. Soc.* **2012**, *134*, 3411−3418. (c) Rodríguez-Morgade, M. S.; Cabezón, B.; Esperanza, S.; Torres, T. *Chem.-Eur. J.* **2001**, *7*, 2407−2413. (d) Marks, T. J.; Stojakovic, D. R. *J. Am. Chem. Soc.* **1978**, *100*, 1695−1705. (e) Day, V. W.; Marks, T. J.; Wachter, W. A. *J. Am. Chem. Soc.* **1975**, *97*, 4519−4527. (f) Bloor, J. E.; Schlabitz, J.; Walden, C. C. *Can. J. Chem.* **1964**, *42*, 2201−2208.

(6) Fukuda, T.; Hata, K.; Ishikawa, N. *J. Am. Chem. Soc.* **2012**, *134*, 14698−14701.

(7) (a) Lim, B.; Margulis, G. Y.; Yum, J.-H.; Unger, E. L.; Hardin, B. E.; Grätzel, M.; McGehee, M. D.; Sellinger, A. *Org. Lett.* **2013**, *15*, 784−787. (b) Cid, J.-J.; García-Iglesias, M.; Yum, J.-H.; Forneli, A.; Albero, J.; Martínez-Ferrero, E.; Vázquez, P.; Grätzel, M.; Nazeeruddin, M. K.; Palomares, E.; Torres, T. *Chem.-Eur. J.* **2009**, *15*, 5130−5137.

(8) Muranaka, A.; Yonehara, M.; Uchiyama, M. *J. Am. Chem. Soc.* **2010**, *132*, 7844−7845.

(9) *Organo Main Group Chemistry*; Akiba, K.-y., Ed.; Wiley-VCH: Weinheim, Germany, 2011.

(10) Kobayashi, N.; Furuyama, T.; Satoh, K. *J. Am. Chem. Soc.* **2011**, *133*, 19642−19645.

(11) (a) Antunes, E. M.; Nyokong, T. *J. Porphyrins Phthalocyanines* **2009**, *13*, 153−160. (b) Breusova, M. O.; Pushkarev, V. E.; Tomilova, L. G. *Russ. Chem. Bull.* **2007**, *56*, 1456−1460. (c) Fox, J. P.; Goldberg, D. P. *Inorg. Chem.* **2003**, *42*, 8181−8191. (d) Li, J.; Subramanian, L. R.; Hanack, M. *Eur. J. Org. Chem.* **1998**, 2759−2767. (e) Gouterman, M.; Sayer, P.; Shankland, E.; Smith, J. P. *Inorg. Chem.* **1981**, *20*, 87−92.

(12) Janczak, J.; Kubiak, R.; Jezierski, A. *Inorg. Chem.* **1999**, *38*, 2043−2049.

(13) (a) Isago, H.; Kagaya, Y. *J. Porphyrins Phthalocyanines* **2009**, *13*, 382−389. (b) Isago, H. *Chem. Commun.* **2003**, 1864−1865. (c) Isago, H.; Kagaya, Y.; Nakajima, S.-i. *Chem. Lett.* **2003**, *32*, 112−113. (d) Kubiak, R.; Razik, M. *Acta Crystallogr.* **1998**, *C54*, 483−485. (e) Isago, H.; Kagaya, Y. *Bull. Chem. Soc. Jpn.* **1996**, *69*, 1281−1288. (f) Kagaya, Y.; Isago, H. *Chem. Lett.* **1994**, *23*, 1957−1960.

(14) Isago, H.; Kagaya, Y. *Inorg. Chem.* **2012**, *51*, 8447−8454.

(15) In this Article, Pcs with nonmetallic elements in their cavities are discussed mainly, and we will call a Pc without an element in its cavity "free-base Pc", while such a Pc is usually called "metal-free Pc".

(16) Kobayashi, N.; Fukuda, T.; Ueno, K.; Ogino, H. *J. Am. Chem. Soc.* **2001**, *123*, 10740−10741.

(17) Satoh, W.; Nadano, R.; Yamamoto, Y.; Akiba, K.-y. *Chem. Commun.* **1996**, 2451−2452.

(18) Kadish, K. M.; Autret, M.; Ou, Z.; Akiba, K.-y.; Masumoto, S.; Wada, R.; Yamamoto, Y. *Inorg. Chem.* **1996**, *35*, 5564−5569.

(19) Kobayashi, N.; Sasaki, N.; Higashi, Y.; Osa, T. *Inorg. Chem.* **1995**, *34*, 1636−1637.

(20) (a) Leznoff, C. C.; Black, L. S.; Hiebert, A.; Causey, P. W.; Christendat, D.; Lever, A. B. P. *Inorg. Chim. Acta* **2006**, *359*, 2690−2699. (b) Mbambisa, G.; Tau, P.; Antunes, E.; Nyokong, T. *Polyhedron* **2007**, *26*, 5355−5364.

(21) The Q-band position in β-^{t}Bu$_4$PcH$_2$ (**10H$_2$**) and **3f** was defined as the center of the Q_{x00} and Q_{y00} bands.

(22) Kobayashi, N.; Ogata, H.; Nonaka, N.; Luk'yanets, E. A. *Chem.-Eur. J.* **2003**, *9*, 5123−5134.

(23) (a) Zimcik, P.; Novakova, V.; Kopecky, K.; Miletin, M.; Kobak, R. Z. U.; Svandrlikova, E.; Váchová, L.; Lang, K. *Inorg. Chem.* **2012**, *51*, 4215−4223. (b) Nesterova, I. V.; Erdem, S. S.; Pakhomov, S.; Hammer, R. P.; Soper, S. A. *J. Am. Chem. Soc.* **2009**, *131*, 2432−2433.

(24) (a) Ikeda, S.; Toganoh, M.; Easwaramoorthi, S.; Lim, J. M.; Kim, D.; Furuta, H. *J. Org. Chem.* **2010**, *75*, 8637−8649. (b) Welsher, K.; Liu, Z.; Sherlock, S. P.; Robinson, J. T.; Chen, Z.; Daranciang, D.; Dai, H. *Nat. Nanotechnol.* **2009**, *4*, 773−780. (c) Casalboni, M.; Matteis, F. D.; Prosposito, P.; Quatela, A.; Sarcinelli, F. *Chem. Phys. Lett.* **2003**, *373*, 372−378.

(25) Nyokong, T.; Antunes, E. In *Handbook of Porphyrin Science*; Kadish, K. M., Smith, K. M., Guilard, R., Eds.; World Scientific: Singapore, 2010; Vol. 7, pp 247−357.

(26) (a) Shimizu, S.; Zhu, H.; Kobayashi, N. *Chem.-Eur. J.* **2010**, *16*, 11151−11159. (b) Cui, L.-Y.; Yang, J.; Fu, Q.; Zhao, B.-Z.; Tian, L.; Yu, H.-L. *J. Mol. Struct.* **2007**, *827*, 149−154. (c) Fukuda, T.; Homma, S.; Kobayashi, N. *Chem.-Eur. J.* **2005**, *11*, 5205−5216.

(27) Wong, C. Y.; Kennepohl, D. K.; Cavell, R. G. *Chem. Rev.* **1996**, *96*, 1917−1952.
(28) (a) Fukuda, T.; Makarova, E. A.; Luk'yanets, E. A.; Kobayashi, N. *Chem.-Eur. J.* **2004**, *10*, 117−133. (b) Kobayashi, N.; Fukuda, T. *J. Am. Chem. Soc.* **2002**, *124*, 8021−8034. (c) Kobayashi, N.; Miwa, H.; Nemykin, V. N. *J. Am. Chem. Soc.* **2002**, *124*, 8007−8020.
(29) Mack, J.; Stillman, M. J. *J. Am. Chem. Soc.* **1994**, *116*, 1292−1304.
(30) Connelly, N. G.; Geiger, W. E. *Chem. Rev.* **1996**, *96*, 877−910.
(31) Gouterman, M. In *The Porphyrins*; Dolphin, D., Ed.; Academic Press: New York, 1978; Vol. *3*, Part A, p 1.
(32) Engel, M. K. In *The Porphyrin Handbook*; Kadish, K. M., Smith, K. M., Guilard, R., Eds.; Academic Press: New York, 2003; Vol. *20*, pp 1−242.